CHAPTER FOUR

Recording Single Motor Proteins in the Cytoplasm of Mammalian Cells

Dawen Cai,[*,†] Neha Kaul,[‡] Troy A. Lionberger,[‡,§] Diane M. Wiener,[‡] Kristen J. Verhey,[*,†,§] *and* Edgar Meyhofer[†,‡,§]

Contents

* Department of Cell and Developmental Biology, University of Michigan, Ann Arbor, Michigan, USA
† Department of Biophysics, University of Michigan, Ann Arbor, Michigan, USA
‡ Department of Mechanical Engineering, University of Michigan, Ann Arbor, Michigan, USA
§ Program in Cellular and Molecular Biology, University of Michigan, Ann Arbor, Michigan, USA

Methods in Enzymology, Volume 475
ISSN 0076-6879, DOI: 10.1016/S0076-6879(10)75004-7

Abstract

Biomolecular motors are central to the function and regulation of all cellular transport systems. The molecular mechanisms by which motors generate force and motion along cytoskeletal filaments have been mostly studied *in vitro* using a variety of approaches, including several single-molecule techniques. While such studies have revealed significant insights into the chemomechanical transduction mechanisms of motors, important questions remain unanswered as to how motors work in cells. To understand how motor activity is regulated and how motors orchestrate the transport of specific cargoes to the proper subcellular domain requires analysis of motor function *in vivo*. Many transport processes in cells are believed to be powered by single or very few motor molecules, which makes it essential to track, in real time and with nanometer resolution, individual motors and their associated cargoes and tracks. Here we summarize, contrast, and compare recent methodological advances, many relying on advanced fluorescent labeling, genetic tagging, and imaging techniques, that lay the foundation for groundbreaking approaches and discoveries. In addition, to illustrate the impact and capabilities for these methods, we highlight novel biological findings where appropriate.

1. Introduction

Biomolecular motors play crucial roles in a large number of cellular functions and are essential components of a carefully orchestrated transport system that maintains the structural and functional properties of cells. Prominent examples of these cellular functions include muscle contraction, vesicular transport in the cytoplasm, formation of the spindle apparatus, segregation of chromosomes during mitosis and meiosis, and powering the beating motion of cilia and flagella. The principal mechanism by which molecular motors accomplish these diverse functions is binding to and moving along cytoskeletal filaments (either microtubules or actin filaments) by transducing the chemical energy available from the hydrolysis of ATP into mechanical work (Block, 2007; Gennerich and Vale, 2009; Schliwa and Woehlke, 2003). Because of the central importance of these mechanisms to biology, a major research effort has been directed toward understanding the molecular mechanism underpinning biomolecular motor function. Spurred by the discovery that the motility of single kinesin motors along microtubules can be reconstituted from purified proteins in cell-free assays (Howard *et al.*, 1989; Vale *et al.*, 1985), a large number of progressively more sophisticated single-molecule techniques, including laser trapping and fluorescence tracking experiments, have been developed to precisely characterize the stepwise movements and forces that molecular

motors generate as they translocate along their respective cytoskeletal filaments (Meyhofer and Howard, 1995; Ray *et al.*, 1993; Svoboda *et al.*, 1993; Visscher *et al.*, 1999; Yildiz *et al.*, 2004). For example, such studies have demonstrated that Kinesin-1 generates maximum forces of about 6 pN and moves processively by taking 8 nm steps. These studies have also shown that kinesin steps over the microtubule lattice parallel to the protofilaments by coordinating the alternating catalytic activity of its two motor domains. While attention of such biophysical work is now shifting toward deciphering the molecular details of how motion and forces are generated and how coordination between the heads is accomplished (Block, 2007), critical questions need to be addressed with regard to the function and regulation of molecular motors in cells in order to understand how different kinesin motors function *in vivo*. Key questions, for instance, include how biomolecular motors move in the crowded cellular environment, how many motors are involved in specific transport processes, how different motors interact in the transport of specific cargoes, how individual motors are directed to specific cellular targets, and how motor activity is regulated within cells. Significant evidence supports the view that relatively few motors, perhaps even single molecules, power many of the transport processes (Laib *et al.*, 2009; Shubeita *et al.*, 2008). Therefore, addressing these challenging problems not only requires analysis of motor function *in vivo*, but also makes it essential to track, in real time and with nanometer resolution, individual motor molecules and their associated cargoes, cytoskeletal filaments, and other proteins in living cells.

Over the last few years, significant technical progress has been made in a number of closely related approaches that make it now possible to follow individual motor molecules in living cells (Cai *et al.*, 2007, 2009; Courty *et al.*, 2006; Kulic *et al.*, 2008; Kural *et al.*, 2005; Nan *et al.*, 2005, 2008). Generally, these techniques rely on labeling motors with one of a rapidly expanding variety of fluorescent labels or with bright, scattering nanoparticles, and on imaging these labels in living cells using low-background confocal, total internal reflection fluorescence, or dark-field microscopy. With the availability of highly sensitive digital cameras, it has also become readily possible to acquire even very faint signals with video resolution, enabling the localization of diffraction-limited spots with subpixel accuracy by fitting appropriate functions to the acquired intensity distributions. As long as it can be assured that individual particles or molecules are being detected and tracked, the position of these spots can be determined with a resolution that is, in principle, only limited by the number of photons that are available to estimate their precise location (Thompson *et al.*, 2002). Using these new approaches, many of which were initially applied to the detailed analysis of motility *in vitro*, recent work has demonstrated the stepwise movement of motors *in vivo*, presented significant support that Kinesin-1 behaves *in vitro* similarly as *in vivo*, and revealed that kinesin

motors differ in their ability to select specific subsets of microtubule tracks in cells (Cai *et al.*, 2007, 2009; Kural *et al.*, 2005, 2007; Levi and Gratton, 2007; Nan *et al.*, 2005, 2008).

In this chapter, we review the methodological foundations, with regard to both the required instruments and biological techniques that have been successfully applied to record single or few motors in living cells. In addition to emphasizing the approaches we have taken in our own work (Cai *et al.*, 2007, 2009), we contrast the advantages and drawbacks of different single-molecule imaging and recording techniques and evaluate how the different characteristics meet the requirements of biological studies of *in vivo* motor function.

2. Basic Principles

Imaging of single biomolecules in live cells is based on a single particle tracking approach where individual molecules are labeled with high contrast or bright, fluorescent particles or labels such that their centroids can be determined with high resolution from image sequences. Beginning with relatively large latex particles *in vitro* (Gelles *et al.*, 1988), the techniques were first successfully applied to *in vivo* studies by characterizing biological processes at the plasma membrane (Barak and Webb, 1982; Cherry, 1992; Kusumi *et al.*, 2005; Sako and Yanagida, 2003; Saxton and Jacobson, 1997; Schmidt *et al.*, 1996). Tracking single molecules inside intact cells has been technically more challenging because of the relatively large cellular autofluorescence and the need to introduce labeled components into cells. By leveraging recent improvements in various (fluorescent) labels, microscopy techniques and CCD detectors, the basic particle tracking approaches have now been successfully adapted to image intracellular events with nanometer resolution (Cai *et al.*, 2007; Courty *et al.*, 2006; Michalet *et al.*, 2005; Nan *et al.*, 2005). Total internal reflection fluorescence microscopy (TIRFM) has played a crucial role in realizing these measurements because of the associated reduction in background fluorescence. In addition, the availability of reliable, low-cost solid-state lasers at multiple wavelengths as efficient and flexible light sources for fluorophore excitation and particle scattering, and sensitive electron-multiplication CCD (EMCCD) cameras have facilitated precise image recording and quantitative analysis of microscopy data that are essential for nanometer-resolution tracking of single molecules. Intriguingly, these same basic single particle tracking principles are now being further extended and developed in a number of super-resolution imaging techniques (like photoactivated location microscopy (PALM) and stochastic optical reconstruction microscopy (STORM)) to circumvent the diffraction-limited performance of the conventional light microscope (see e.g., Huang *et al.*, 2008).

3. Labeling Molecular Motors for *In Vivo* Observations

Perhaps the most critical and challenging step in experimentally analyzing the cellular function and molecular mechanisms of motors in living cells is that light-emitting or light-scattering molecules or particles have to be attached to the motors of interest to track their movement and characterize their interactions with other cellular components. For high-resolution tracking (temporal and spatial) these particles need to be optically bright and photostable, yet neither the label nor the labeling procedure should alter or influence the functional or physiological properties of the motor or other relevant cellular constituents. The labeling should be highly specific to individual molecules and not induce oligomerization or clustering of labels and molecular motors. Also, the simultaneous labeling of molecular motors, cytoskeletal tracks, cargoes, scaffolding proteins, linkers or regulatory components with multiple, distinguishable (e.g., spectroscopically distinct) fluorophores is highly desirable to study the molecular mechanisms of biomolecular motor-based transport. Clearly, these are conflicting criteria that need to be carefully balanced, given the biological question at hand. To date, there is no single best label, and not surprisingly, the development of new labels is attracting much attention (see e.g., Chang *et al.*, 2008; Johnsson, 2009; Shaner *et al.*, 2005, 2008). Below, we discuss various labeling and single particle tracking approaches (ranging from organelle labels to single organic fluorophores) that have been employed for studying (single) motors in live cells.

3.1. Organelles as labels for cytoplasmic motors

The discovery of kinesin (Kinesin-1) as a motor for fast axonal transport is explicitly linked to the study of organelle transport (Brady, 1985; Vale *et al.*, 1985). In fact, organelle transport had been investigated for many years prior to the discovery of kinesins, leading to important technical advances like video-enhanced differential interference contrast (DIC) (Allen *et al.*, 1981; Salmon and Tran, 1998). It is therefore not surprising that organelles, which are relatively large in size and are known to be transported by various motors, have been utilized to analyze the movement of motor molecules in live cells. A relatively simple, but powerful approach is to take advantage of the natural labeling of melanosomes (melanin-containing, pigmented organelles in melanophores), which can be visualized directly in bright-field microscopy due to the high contrast between the melanosomes and the background of the cytoplasm (Gross *et al.*, 2002; Kural *et al.*, 2007; Levi *et al.*, 2006). In a recent study, Kural *et al.* (2007) were able to use this approach and track the position of individual melanosomes with $\sim$2 nm spatial and 1.1 ms

temporal resolution by fitting a 2D Gaussian function to the reversed (or negative) bright-field image of melanosomes. This method (bFIONA or bright-field FIONA) is an extension of the previously developed, fluorescence-based FIONA (fluorescence imaging with one-nanometer accuracy, see Section 4.5) (Yildiz *et al.*, 2003). Since it is now quite well established that myosin V, cytoplasmic dynein, and Kinesin-2 motors are all located on and involved in the movement of these organelles in melanophores, selective depolymerization of either actin filaments or microtubules (with latrunculin B or nacodazole, respectively) reduces motor interactions to microtubule-based dynein and kinesin motors or actin filament-based myosin V. Using this approach, the authors were able to characterize the anterograde and retrograde stepping ($\sim$8 nm) of Kinesin-2 and dynein along microtubules, and they showed that myosin V transported organelles along actin filaments in 35-nm increments. Most intriguingly, in the presence of both microtubules and actin filaments, the melanosomes moved along actin filaments and microtubules nearly simultaneously, indicating that clearly distinct diffusion events for switching from one cytoskeletal filament to the other are not necessary.

To track the motion of molecular motors and organelles in nonmelanophore cells, approaches have been developed to intensely label organelles for single particle tracking. The movement of peroxisomes by kinesin and dynein motors was recorded by Kural *et al.* (2005) and subsequently Kulic *et al.* (2008) by constitutively expressing EGFP (enhanced green fluorescence protein) with a peroxisome targeting sequence in cultured *Drosophila* S2 cells, which leads to the accumulation of a large number of EGFP molecules in these organelles. Because of the large number of photons that can be collected from the labeled peroxisomes, it is possible to determine the centroid location of labeled, single peroxisome particles with about 1 ms and 1.5 nm accuracy. Nan *et al.* (2005) followed the same basic strategy and introduced bright, fluorescent quantum dots (QDs, see Section 3.2) into endocytotic vesicles of human lung cancer (A549) cells by exposing the cells directly to streptavidin and biotin–polyarginine-coated QDs. Typically, 5–30 QDs were taken up into individual endocytotic vesicles. Because of their bright fluorescence signals, these labeled endocytotic vesicles can be tracked with high temporal ($\sim$0.3 ms) and spatial ($\sim$1.5 nm) resolution following the same single particle or centroid tracking approach outlined above. The same group has now extended this work (Nan *et al.*, 2008) to even higher resolution, by replacing the QD labels with 100–150-nm-diameter gold nanoparticles. Such large gold particles generate very strong scattering signals when excited by laser excitation and objective-based dark-field microscopy, and they are also very photostable. Using this gold nanoparticle system, it is now possible to follow organelles *in vivo* in the cytoplasm at 25-μs and 1.5-nm resolution. With this improved methodology, Nan *et al.* present evidence that cytoplasmic dynein takes 8, 12, 16, 20, and 24-nm steps over the full range of physiologic velocities, while kinesin steps consistently in 8-nm intervals.

3.2. Quantum dots

QDs are semiconductor nanocrystals with highly desirable fluorescence properties for tracking motors inside live cells (see e.g., Alivisatos *et al.*, 2005; Michalet *et al.*, 2005). QDs are about 20-fold brighter, and vastly more photostable (by orders of magnitude) than organic dye molecules and fluorescent proteins. To ensure solubilization and functionality, the nanocrystal core of commercially available QDs is encapsulated by a shell and polymer-coat to link a variety of bioconjugation molecules (like streptavidin or antibodies) to the QD surface. Thus, the size of these particles typically falls into the range of 15–20 nm. The disadvantages to motor-QD couplings are that the linked molecules must be generated *in vitro* and then introduced into cells and that the stoichiometry of motors on an individual QD cannot be controlled. The physical size of the QD, which is often larger than the actual motor domain under investigation, can also be a concern.

Courty *et al.* (2006) directly attached truncated, biotinylated *Drosophila* Kinesin-1 motor domains to QDs at two stoichiometries, confirmed motility of the kinesin-QD conjugates in *in vitro* motility assays, and then loaded the kinesin-QDs into the cytoplasm of HeLa cells with a cell loading technique that is based on osmotic lysis of pinocytotic vesicles. Alternatively, microinjection of the QDs into the cells was used, but Courty *et al.* (2006) report that the pinocytotic loading technique proved to be more reliable. Kinesin-labeled QDs located uniformly in the cytoplasm of cells but were excluded from the nucleus. Moreover, Courty *et al.* showed that the labeled particles were not aggregating, by using fluorescence intermittency and mixtures of QDs emitting at 605 and 655 nm as signatures for possible aggregation of the QDs. By means of conventional fluorescence microscopy, they observed (as expected from the labeling ratios) both diffusing QDs and QDs exhibiting linear trajectories. Analysis of the linear trajectories showed that single QDs were transported at a velocity of ~ 0.6 μm/s and over distances of about 1.7 μm, in agreement with single-molecule *in vitro* properties of Kinesin-1 from *Drosophila*. More recently, Nelson *et al.* (2009) developed a similar QD-based method and successfully tracked the movement of myosin Va motors in COS cells. Interestingly, their work implies that myosin Va motors move processively and at the same time undergo a random walk through the dense and randomly oriented cortical actin network.

3.3. Organic fluorophores and genetic tags

With the systematic development of an array of fluorescent proteins and genetic tags, we now have available a large library of fluorescent labels that offer the advantage of being genetically (and therefore precisely) attached to the protein of interest with exactly known stoichiometries (Davidson and Campbell, 2009; Shaner *et al.*, 2005, 2008; Snapp, 2009). In addition, these

labels make it readily feasible to precisely tag multiple components of the cellular transport system, such that it is finally becoming technically possible to address many of the outstanding questions in cell biology and biophysics regarding molecular motor function *in vivo*.

Our own work on the molecular mechanism and functional regulation of kinesin-based, cellular transport requires highly specific labeling of different motors, cargoes, and cytoskeletal components. Fluorescent proteins are an excellent choice for genetically labeling the protein of interest as they are available in many colors and can be added to N- or C-termini or even to internal segments of protein. The disadvantage to fluorescent proteins is their relatively low brightness and high photobleaching rate. To enable the imaging of fluorescently tagged kinesin motors despite the relatively high autofluorescence levels in the cytoplasm of cells, we developed a three-tandem monomeric Citrine (mCit) label that, in combination with sensitive TIRFM, proved to be sufficiently bright to track the movement of individual kinesin motors in live cells with the required resolution (Cai *et al.*, 2007). Recently, we have also been able to extend this approach to simultaneous two-color observations (Cai *et al.*, 2009). These technical developments have already enabled important biological discoveries and allowed us to determine, in contrast to earlier studies tracking the movement of entire organelles (Kural *et al.*, 2005), that individual Kinesin-1 motors move similarly inside cells as they do *in vitro*. In addition, we have gathered significant support for a model in which different kinesin families distinguish specific microtubule populations to enable targeting of transport events to distinct subcellular domains (Cai *et al.*, 2009).

Alternative genetic labeling methods for *in vivo* protein studies, including a small tetracysteine–biarsenical system (Griffin *et al.*, 1998) and a number of enzyme-based protein tags (e.g., acyl carrier protein, alkylguanine-DNA-alkyltransferase; see e.g., Chang *et al.*, 2008; Johnsson, 2009; Keppler *et al.*, 2003) have been developed during the last decade. In these methods molecular tags (ranging from as few as six amino acids to 10–30 kDa enzymes) are genetically fused to the proteins of interest and (co-)expressed in cells. Subsequently, specific labeling molecules, some of which are membrane permeable, are introduced into the cytoplasm to bind to the genetic tags and fluorescently label (or otherwise functionalize) the fusion proteins. Clearly, these labeling approaches are highly flexible, and the tags and labels can be very small in comparison to fluorescent proteins (e.g., the membrane-permeable biarsenic FlAsH and ReAsH dyes require only the inclusion of the tetracysteine motif Cys-Cys-X-X-Cys-Cys, where X is a noncysteine amino acid, within a protein of interest). Consequently, these labeling approaches hold significant promise for the development of refined labeling techniques that are necessary to investigate the mechanistic interactions between motor molecules and other components of the cytoskeleton, as demonstrated by *in vivo* and single molecule *in vitro* experiments

(see e.g., Gaietta *et al.*, 2002; Giepmans *et al.*, 2006; Park *et al.*, 2004). In addition, these labeling approaches can also be used for affinity purification, fluorophore-assisted light inactivation, pulse-chase labeling, or correlative electron microscopy (see Giepmans *et al.*, 2006). Experiments going beyond simply tracking the movement of motors in cells would, however, benefit significantly from additional developments such as probes with additional biochemical specificities and higher quantum yields, as well as techniques capable of further reducing cellular background signals.

4. Instrumentation for Tracking Single Motors *In Vivo*

The instrumentation required for recording the movement and molecular interactions of single molecules in the cytoplasm of cells is largely dictated by the labeling strategies and resolution requirements. TIRFM has emerged over the last 15 years or so as one of the preferred microscopy techniques for single-molecule *in vitro* and *in vivo* studies, largely owing to significant reduction of background fluorescence and the relative simplicity, ease of use, and commercial availability of the required instrumentation (Axelrod, 2003; Funatsu *et al.*, 1995; Roy *et al.*, 2008; Simon, 2009; Walter *et al.*, 2008). Principally, the improved sensitivity over conventional epi-fluorescence is achieved by selectively exciting only a very small portion of the sample at the glass–solution interface of the experimental chamber via the evanescent wave that is generated in total internal reflection. The intensity of the evanescent wave declines exponentially over a depth of only ~50–150 nm, depending on the exact angle of incidence of the reflected light and the local refractive indices. To image deeper inside the cytoplasm beyond the immediate cell surface, others and we have reduced the angle of TIRF illumination to below the critical angle to generate a highly inclined and laminated optical sheet (see e.g., Cai *et al.*, 2007, 2009), described as HILO microscopy by Tokunaga *et al.* (2008). To improve the stability, sensitivity, versatility, and affordability of our instrument, we have constructed an objective-based TIRF microscope with multicolor excitation capabilities by integrating the appropriate laser sources, optical components, a dual-view imager, and a CCD camera into a commercial, inverted microscope system (Zeiss Axiovert 135TV). In fact, in our opinion, a TIRF microscope is a single-molecule instrument that can be designed and constructed with relative ease, and there are many excellent and recent reviews (listed in the above citations) on the subject. Here we highlight some aspects of instruments that may be relevant with regard to *in vivo* single motor imaging work.

4.1. Multicolor TIRF illumination

The simultaneous excitation of distinct fluorophores for multicolor TIRF microscopy requires careful selection of fluorophores, excitation wavelengths, and optical components to efficiently collect the maximum possible signals. Given our requirement to simultaneously image at least two fluorescent proteins with maximum sensitivity, we need to precisely adjust the excitation intensity of each laser source such that the photobleaching rate and relative intensity of the different fluorescent labels are carefully optimized for a given experiment. We achieved this goal by coupling the beams of multiple laser sources (488, 532, and 593 nm) into one single-mode fiber (Fig. 4.1A). This configuration also enables the simultaneous alignment of all laser lines during the experiment. The intensity of each laser (wavelength) is modulated by rotating a $\lambda/2$ waveplate (Fig. 4.1A, HWP) to align the orientation of the axis of polarization with a polarizing beam splitter (Fig. 4.1A, PBS) prior to coupling the light into a single-mode fiber. The laser wavelengths are combined by choosing appropriate dichroic mirrors to reflect shorter wavelengths and transmit the longer ones. The transmitted and reflected laser beams are then colocalized and coupled into a single-mode fiber that transmits the excitation light to the TIRF microscope. Coupling the light into single-mode fibers spatially filters the beams into a TEM_{00} Gaussian profile and delivers the laser light to the microscope system from remotely housed laser sources. In this system, the intensity from the lasers can be independently and precisely adjusted, and coupling efficiencies of $>50\%$ are maintained throughout by coupling the light into fibers with angle polished ends using adjustable focus and fiber coupling lenses (Fig. 4.1A, FCL) with carefully chosen, wavelength-specific focal lengths. This arrangement also requires that the light emitted from each laser-specific single-mode fiber be collimated prior to coupling all wavelengths into the same fiber to avoid damaging the dichroic mirrors (Fig. 4.1A, D1 and D2) by high power densities. Additionally, fibers with adjustable focus are necessary such that each wavelength can be independently focused to achieve precise coupling and high efficiencies when combining them into a single fiber. Moreover, when using planar optics ($\lambda/2$ waveplate and polarizing beam splitter), a slight ($<2^\circ$) rotation of the optics in opposing directions (for a net zero change in the beam path) will reduce back-reflections and any associated interference.

An alternative, more sophisticated approach to a multiwavelength excitation system can be accomplished by the approach outlined by Ross *et al.* (2007). If more than three excitation wavelengths are required, available multichroic beamsplitters are significantly limited in terms of the transmission ranges, thereby reducing collection efficiencies in the emission bands. This limitation was overcome by using a multiline laser, an acousto-optical tunable filter, and an acousto-optical, tunable beam splitter, to rapidly select

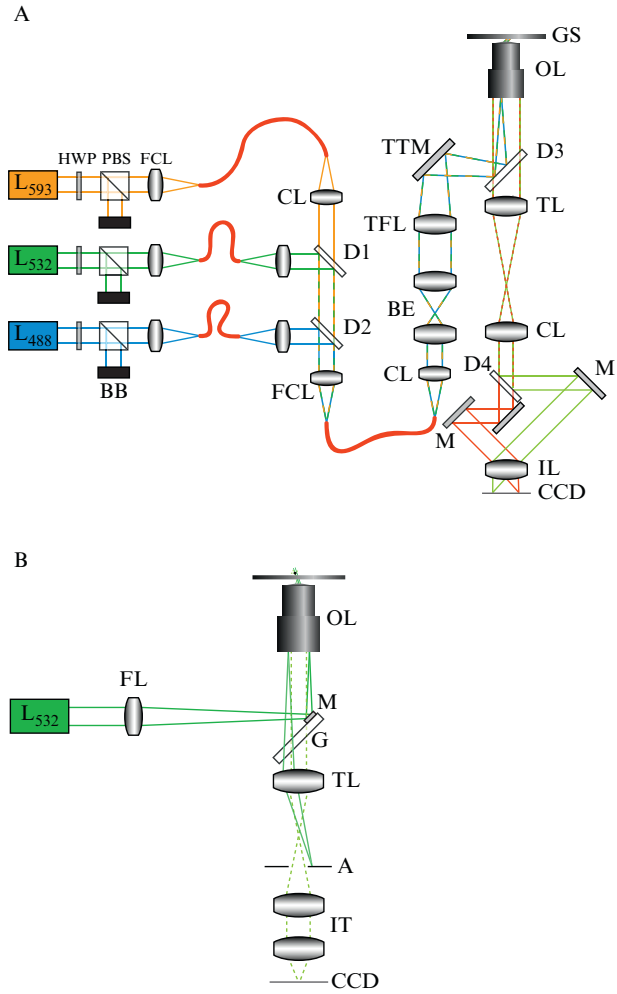

Figure 4.1 Microscope setups for tracking single motor proteins. (A) Tri-color TIRFM. Multicolor excitation is provided by three laser sources with wavelengths of 488 nm (Melles Griot Ar^{+}, solid blue path), 532 nm (CrystaLaser DPSS, solid green path), and 593 nm (CrystaLaser DPSS, solid orange path). The output power of each laser is independently modulated by rotating a $\lambda/2$-waveplate (HWP, Tower Optics) to adjust the polarization axis with respect to a polarizing beam splitter (PBS, Linos Photonics) which divides the light between a beam block (BB) and a lens (FCL) which in turn couples the light into a 3-μm single-mode fiber (Oz Optics). After exiting the fiber, the laser light is collimated (CL) and the three wavelengths are colocalized using dichroic mirrors (D1, D2, Chroma Technology and Semrock). This combined, multiwavelength beam is coupled into a 3-μm single-mode fiber (Oz Optics) to easily interface with the TIRF microscope. A collimation lens (CL) and a telescope (BE) expand the beam to the appropriate diameter such that it can be focused with the TIR focusing lens (TFL) and directed with a kinematic tip-tilt mirror (TTM, Newport

and deflect the excitation wavelengths in fast sequence toward the sample while maintaining broadband spectral transmission suitable for all fluorophore emission profiles (Ross *et al.*, 2007).

4.2. Dark-field excitation to track nanoparticles

Alternative single particle tracking methods capable of enabling both high temporal bandwidths and high spatial resolution in live cells include using gold nanoparticle labels or plasmon coupling between two gold nanoparticles. However, both techniques require specialized excitation illumination. Utilizing the scattering signal from gold nanoparticles is highly advantageous because their photostability allows high excitation intensities and consequently high temporal resolution and long observation times. Molecular motors labeled with gold nanoparticles have been used in tracking experiments *in vitro* (Dunn and Spudich, 2007) and *in vivo* (Nan *et al.*, 2008), using dark-field illumination with laser excitation to achieve 25-μs temporal resolution and 2-nm spatial resolution (Braslavsky *et al.*, 2001; Nan *et al.*, 2008; Nishiyama *et al.*, 2001). The optical path of objective dark-field illumination is similar to objective-based TIRF microscopy (Fig. 4.1B). However, the dichroic mirror in TIRF microscopy is replaced by a small mirror (Fig. 4.1B, M) that is $\sim$5 mm diameter and attached to a glass substrate. By carefully aligning the excitation source, this mirror reflects the incoming light into the back-focal plane of the microscope objective. The collected, scattered light passes through the glass substrate and is measured with a CCD camera or photodiode. Because the imaging planes of the scattered light (which is necessarily divergent as it is emitted from the specimen) and reflected light (which is collimated) are different, the reflected illumination can be effectively blocked by an appropriately placed aperture (Fig. 4.1A and B). Another experimental approach to measuring distances within live cells, plasmon coupling (Jun *et al.*, 2009;

Ultima U100) and an appropriate dichroic mirror (D3, multiband laser dichroic from Chroma Technology) into the back focal plane of the TIRF microscope objective. The TTM allows precise alignment of the laser excitation sources for TIRF. Fluorescence emission signals (here shown as light and dark gray paths) are transmitted through the dichroic mirror (D3) and imaged by the tube lens (TL). A custom dual-view system splits (via dichroic mirror D4) the image into two-color components and projects them side-by-side (with mirrors (M) and lens (IL) onto the sensor of a single EMCCD camera (Photometrics 512B Cascade). (B) Objective Dark-field. A small mirror (M) attached to an antireflection-coated glass substrate (G) reflects the illumination laser beam (solid line) into the back-focal plane of the microscope objective lens (OL). The scattered light from gold nanoparticles (dashed line) is collected by the objective, passed through the glass substrate, and is imaged by the TL and a magnifying imaging telescope (IT) onto a CCD. Back-reflected illumination light from the glass coverslip is blocked by an aperture (A) to increase the signal-to-background ratio.

Rong *et al.*, 2008), maintains the advantages of dark-field illumination and is additionally capable of reporting the distance between two gold nanoparticles (to within 15 nm *in vivo*) by measuring their spectral response (Reinhard *et al.*, 2005). Despite the advantages of gold nanoparticle tracking, large gold nanoparticles must be used (40–200 nm in diameter) to achieve the desired temporal and spatial resolution, which limits their applicability to many biological problems.

4.3. Recording single-molecule events

The most versatile and widely used devices for capturing images of single molecules *in vivo* are digital CCD cameras. They offer high quantum efficiency over a broad range of wavelengths, pixel-limited resolution, and a wide dynamic signal range. However, the readout noise from CCD chips is significant when dim, single-molecule events are imaged. Moreover, following the above discussion on labels for observing single motor events in cells, these measurements will always be limited by the number of photons emitted from a given label and collected by the CCD. Specifically, the spatial and temporal resolutions are both highly dependent on the number of collected photons, and therefore are inversely related. During recent years, the development of EMCCD sensors by E2V and Texas Instruments has led to significant technical improvements that enabled the development of cameras with $>90\%$ quantum efficiency in the wavelength range from 500 to 700 nm (now available from a number of camera manufacturers, including Andor, Roper Scientific, and Hamamatsu). The on-board gain function of these EMCCD cameras circumvents previous limitations in the readout noise of CCD devices to achieve single photon sensitivity. The cameras also feature high readout rates (10–12 MHz) leading to full frame transfer rates of >30 Hz for 512×512 images and frame rates in excess of 1 kHz for smaller frame transfer chips and subarrays. In our recent work, we used a Photometrics 512B Cascade model from Roper Scientific with success (Cai *et al.*, 2007, 2009). This camera is based on a back-illuminated, frame transfer CCD device (CCD97 from E2V) with a 512×512-pixel imaging array, on-chip electron multiplication gain, and the highest available quantum efficiency of $>90\%$. The camera is thermoelectrically cooled to -30 °C, supports fast readout at a rate of 10 MHz, and is a considerable improvement over intensified CCD cameras that we used in past work. In general, EMCCD cameras have played a critical role in enabling high-resolution single particle tracking experiments (highlighted by FIONA, Yildiz *et al.*, 2003, and recent super-resolution microscopy; see e.g., Betzig *et al.*, 2006; Huang *et al.*, 2008).

To further increase the temporal resolution in motor tracking experiments with large gold nanoparticles (100–150 nm), Nan *et al.* (2008) developed a novel detection strategy that uses dark-field microscopy and a high-bandwidth quadrant photodiode to determine the centroid of the gold particles (Nan *et al.*,

2008). Any displacement of a single gold nanoparticle detected (in 2D) with the photodiode is immediately offset via a feedback loop-based adjustment of a piezoelectric sample stage. Because of the high bandwidth of the photodiode and the bright scattering signal from the gold nanoparticle, this unique detection method achieves a spatial (1.5 nm) and temporal (40 kHz) resolution that is not possible with current EMCCD cameras.

4.4. Dual channel image recording

Dual-color imaging for truly simultaneous acquisition of images from two fluorophores can be achieved by splitting the emitted fluorescence signals for side-by-side capture by a single camera and image processor. This can be achieved through either an internal configuration, wherein the beam splitter is inserted between the objective and eyepiece, or an external configuration, wherein the beam splitter is placed outside the microscope before the CCD camera (Kinosita *et al.*, 1991). Commercial dual-view attachments for microscopes (such as those offered by Hamamatsu, Optical Insights, and Photometrics) are designed based on the above-mentioned configurations. Although they are equipped with exchangeable filter cubes, the position of the lenses is not adjustable to independently focus each channel. Since the microscope objectives used for TIRFM typically have extremely high numerical apertures (NAs), it is impossible to achieve practical, apochromatic designs over the full visible spectrum (i.e., the two images may not be parfocal). For example, when we simultaneously imaged mCit and mCherry fusion proteins in our TIRF system with a 1.45 NA, 100× α-Plan-Fluar (Zeiss) and an Optical Insights Dual-View system, the two images were noticeably focused to different imaging planes. As a solution to this problem, we inserted a long focal distance "contact" lens (focal length ~150 mm) into the light path of the longer emission wavelength channel to further converge the beam and achieve critical focus of both images in the same plane.

4.5. Postimage processing

Originally, particle tracking methods were developed for the analysis of imaging data from *in vitro* motility experiments. By employing contrast-enhancing techniques such as DIC microscopy, the centroid of a reporter particle (submicron latex beads) could be determined with subpixel resolution using methods such as image cross-correlation to achieve a resolution of 1–2 nm with an acquisition rate of 30 Hz (Gelles *et al.*, 1988). With the use of new fluorescent labels and imaging methods, techniques emerged to also track fluorophore labeled molecules with high spatial and temporal resolution. Most current localization techniques take advantage of the fact that the point spread function (PSF) of a diffraction-limited fluorescent particle in a conventional fluorescence microscope can be well approximated

by a 2D Gaussian. Fitting single, diffraction-limited spots produced by fluorescent molecules with a 2D Gaussian function, popularly known as FIONA, has been used widely to characterize the single-molecule behavior of molecular motors both *in vitro* (Yildiz *et al.*, 2003, 2004) and *in vivo* (Courty *et al.*, 2006; Kural *et al.*, 2005, 2007, 2009). FIONA has proved capable of localizing a target molecule to within 1.5 nm with millisecond resolution, and has recently been extended to colocalize two fluorescent dyes, each with unique spectral characteristics, labeling a single DNA. By spectrally discriminating the dyes prior to imaging onto a single CCD camera, this two-color FIONA, also known as SHREC (single-molecule high-resolution colocalization), has been demonstrated to localize two fluorophores within 10 nm of each other (Churchman *et al.*, 2005).

4.6. Microscope accessories

Many standard mechanical microscope stages and stepper designs for sample manipulation employ gears for x–y positioning. Because such systems exhibit significant backlash, it is highly advisable to replace such systems with a precision, flexure hinge-based, piezoelectric design as available from several manufacturers (e.g., Physik Instrumente, Mad City Labs, Queensgate, Jenoptik). For studies aimed at retrospectively correlating live-cell imaging with immunolabeling of fixed cells, the ability to reproducibly locate the same cell in the same orientation is desirable. We have achieved this by designing a specialized, compact mounting frame to which tissue culture dishes with optical quality cover glasses are temporarily glued. The two perpendicular edges of the frame are accurately mounted on the microscope stage with the aid of three alignment pins that allow reproducible mounting with $\sim$1-μm accuracy. The mounting frame and culture dish are held in place with microscope sample clips.

A critical aspect for live-cell imaging is to maintain physiological conditions for cells on the microscope stage. Temperature, humidity, CO_2 and O_2 tension, and the pH of the buffer should be sustained once cells are transferred to the microscope stage. This may be best achieved through the use of a micro CO_2 incubator and a small, objective-based, electrical heating system (Ince *et al.*, 1983) during high resolution, vibration, and drift-sensitive measurements, rather than a large, commercial incubator system.

5. Detailed Experimental Procedures

As outlined above, the specificity of labeling and the nondisruptive introduction of motor molecules into the cytoplasm are critical to the experimental analysis of single motor molecules in live cells. Courty *et al.*

(2006), and more recently Nelson *et al.* (2009), followed the general approach used in *in vitro* studies and conjugated purified motor proteins to QDs (Courty *et al.*, 2006; Nelson *et al.*, 2009) and introduced them into the cells by pinocytosis and osmotic lysis (Okada and Rechsteiner, 1982). We prefer to use genetic tagging with fluorescent proteins to achieve the most physiological *in vivo* imaging conditions. Here we outline the methodological details that allowed us to track single kinesin motors in cells with fluorescent protein-based genetic tags.

5.1. Fluorescent protein-labeled motors

Transient expression of fluorescent protein-labeled molecules is used extensively in cell biology to study protein functions in living mammalian cells (Giepmans *et al.*, 2006). This approach also offers the distinct advantage that expression and synthesis via the cell's own molecular machineries ensures proper folding and modifications of the kinesin motor and other cytoskeletal proteins. To generate sufficiently bright labeling, we engineered a three-tandem copy of mCit as label and fused it to Kinesin-1 (Cai *et al.*, 2007). This method was subsequently leveraged for two-color TIRF experiments (Cai *et al.*, 2009) in which we simultaneously imaged single kinesin motors and cytoskeletal microtubule tracks (Fig. 4.2).

5.2. Fluorescent protein fusion plasmids

As a bright variant of the jellyfish *Aequorea victoria* green fluorescent protein (GFP), mCit was chosen as fluorescence tag. Its longer emission wavelength (peak emission 527 nm) allows for high-efficiency emission collection while

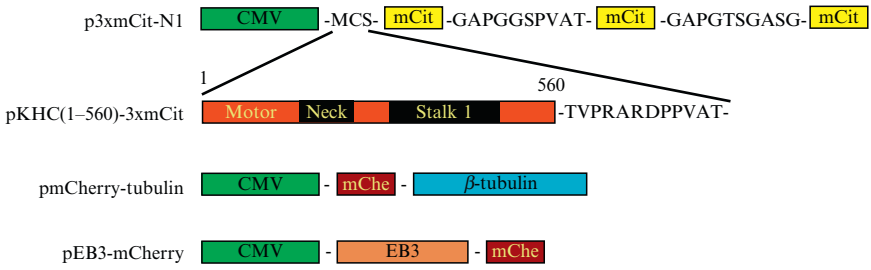

Figure 4.2 Design of plasmids for transfection of mammalian cells with fluorescent fusion proteins. The vector p3×mCit-N1 was constructed based on pEGFP-N1 backbone (Clontech) and contains three-tandem mCit fluorescent proteins proceeded by a multiple cloning site (MCS). A truncated, constitutively active, dimeric Kinesin-1 motor domain (heavy chain amino acids 1-560, KHC1-560) was then inserted in frame into the (MCS). The *β*-tubulin and EB3 genes were amplified by PCR and inserted in frame into the pmCherry-C1 and pmCherry-N1 vectors, respectively. Mammalian expression of these constructs is under the control of the CMV promoter.

using a 488-nm argon ion laser for excitation. To increase labeling brightness, a vector containing three-tandem copies of mCit (p3×mCit-N1) was created by PCR using the EGFP-N1 vectors (Clontech, Palo Alto, CA) as a backbone. Ten amino acid linkers (GAPGGSPVAT and GAPGTSGASG) connect the three copies of mCit (Fig. 4.2). In our initial studies, the three mCit polypeptides were encoded by the same nucleotide sequence. Occasional and random mutation or recombination of this sequence, presumably due to the three identical coding sequences, led us to redesign the 3×mCit tag such that the three mCit polypeptides are coded by different nucleotide sequences. Constitutively active Kinesin-1 motors are generated by deletion of the autoinhibitory tail domain of the kinesin heavy chain (KHC) subunit. These motors, KHC(1-891) or KHC(1-560), are fused to the N′-terminus of p3×mCit. Our initial studies utilized a 12-amino acid linker (Fig. 4.2, TVPRARDPPVAT) between KHC and the mCits, although shorter linker sequences are sufficient. We used the CMV promoter because its high expression efficiency made it possible to achieve proper expression levels for single-molecule imaging in just a few hours after transfection (Fig. 4.3). However, if single-molecule imaging over days is preferred, a truncated CMV promoter (Watanabe and Mitchison, 2002) or β-actin promoter (Dieterlen *et al.*, 2009) can be used for driving expression at lower levels over long periods. For two-color TIRF experiments, other polypeptides of interest can be labeled with other fluorescent proteins. In our experiments, we used mCherry as a second fluorescent protein (Shaner *et al.*, 2005). mCherry was fused to the α-tubulin subunit to label all microtubules or to end-binding protein 3 (EB3) to label dynamic microtubules. mCherry-tubulin and EB3-mCherry were generated by inserting α-tubulin and EB3 PCR products in frame to the C′- and N′-termini of mCherry, respectively (Fig. 4.2).

5.3. Cell culture

Fibroblast cells (e.g., COS cells) are ideally suited for live-cell imaging due to their hardiness and tolerance of exogenous gene expression. They attach readily to glass coverslips and their flat morphology is particularly suited for single-molecule microscopy because of the reduced background fluorescence. Other cells lines with flat morphology, such as PtK2, MRC-5, and LLC-PK1, are also well suited for live-cell imaging. COS cells are routinely cultured in 10-cm plates (Falcon or Corning) in growth medium (10% (v/v) FBS, 1% (w/v) L-glutamine, in DMEM medium) at 37 ° C in an incubator with 5% (v/v) CO_2. Normally, COS cells divide every 24 h when cultured at 10–90% confluence. For passaging or splitting cells for transfection, 70–90% confluent cultures are used. The media is first aspirated and the cells are washed once with 2 ml of sterile PBS buffer (pH 7.4). After removing the PBS wash buffer, 2 ml of 0.25% (w/v) trypsin is added to

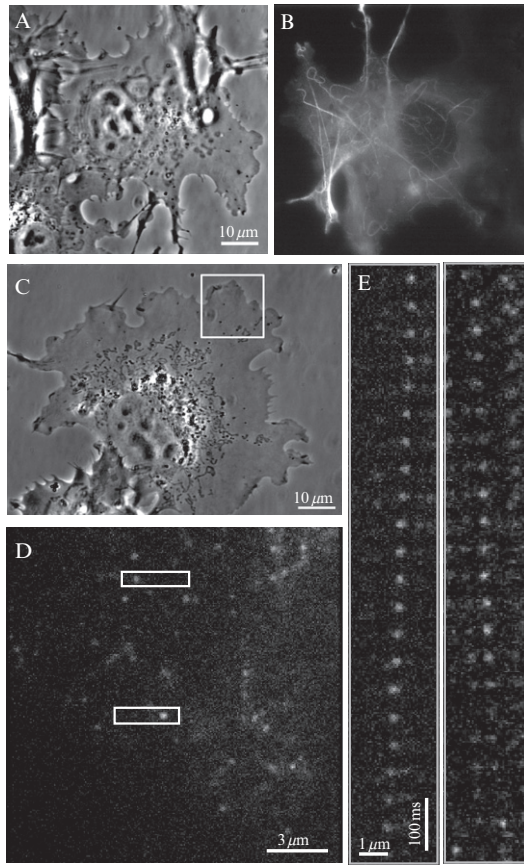

Figure 4.3 Tracking single kinesin motors in COS cells transfected with kinesin-3×mCit fusion protein. (A) Phase-contrast image of a cultured COS cells. (B) Epi-fluorescence image of a transfected COS cell expressing kinesin-3×mCit fusion protein at a high level. At a low expression level (C) the cell's periphery is well-suited for tracking single kinesin motors (white box, magnified view in (D)). A kymograph analysis of two single molecule events (white boxes in (D)) is shown in (E), indicating that both motors move processively at physiological rates (0.6 μm/s).

the plate. When the cells start to detach from the culture dish (2–10 min, depending on temperature), 2 ml of fresh culture medium is added to quench the trypsin. Cells should be completely separated from each other by pipetting before counting with a standard hemocytometer. 10^5 cells are added with 2 ml of fresh culture medium to a 35-mm cell culture dish containing a 25 mm × 25 mm, #1.5 cover glass (MatTek Corporation). The cells are returned to the incubator and allowed to settle for 6–20 h. Before transfection, the cells should be checked by phase contrast

microscopy to confirm that most cells are attached to the cover glass and exhibit the typical flat morphology. Cells should reach ~50% confluence before transfection and should not be over 90% confluent at the time of imaging.

5.4. Transient expression of fluorescent protein-labeled kinesin motors and microtubule markers

To initiate the transient expression of labeled kinesin motors, we prefer TransIT-LTI (Takara Mirus Bio, Madison, WI) or Fugene6 (Roche) and follow the manufacturer's protocols.

1. Briefly, the culture medium (2 ml) in the 35-mm culture dish is exchanged 2–4 h before transfection. The transfection reagent is then used following the manufacturer's protocol.
2. The transfection reagent (stored at −20 °C) is warmed to room temperature 10 min before use. To transfect the kinesin-FP motor alone, 3 μl of gently vortexed transfection reagent is suspended thoroughly in 100 μl of serum-free Opti-Mem media (Invitrogen), followed by 0.5 μg of KHC-3×mCit plasmid DNA (DNA concentration should be ~0.5 μg/μl).
3. The transfection mixture is then incubated at room temperature for 20 min before adding it evenly to culture dish. The transfected cells are returned to the incubator and allowed to express for 4–10 h to achieve low expression levels for single-molecule imaging (Fig. 4.3).
4. To simultaneously image kinesin motors and dynamic plus ends of microtubules, 0.5–1 μg of EB3-mCherry and 0.5 μg of KHC-3×mCit plasmid DNA are mixed prior to adding them to the Opti-MEM transfection reagent mixture.
5. To simultaneously image kinesin motors and all microtubules, 1 μg of mCherry-tubulin is transfected into COS cells and expressed for 24–30 h to allow mCherry-tubulin to be incorporated into all the microtubules. The same cells are then retransfected with 0.5 μg of Kinesin-3×mCit plasmid DNA and allowed to express for an additional 4–10 h.

5.5. Recording and analyzing single-molecule *in vivo* events

To image single molecules *in vivo* in transfected COS cells, we proceed as follows:

1. Transfected cells are carefully rinsed with 37 °C Ringers solution (10 m*M* HEPES/KOH, 155 m*M* NaCl, 5 m*M* KCl, 2 m*M* $CaCl_2$, 1 m*M* $MgCl_2$, 2 m*M* NaH_2PO_4, 10 m*M* glucose, pH 7.2). Cells are maintained in Ringers buffer during imaging.

2. Immersion oil should be applied to the high NA TIRF objective before the 35 mm culture dish is mounted on the heated microscope stage. A temperature-controlled objective collar is preferred to keep the cells at 37 °C.
3. Cells with proper expression levels for imaging are then searched for under conditions meant to minimize excessive photobleaching. To do this, low excitation laser power (~0.03 mW) is used at this stage. Cells with high expression levels usually show significant labeling (decorating) of microtubules with kinesin motors, which can be identified easily by direct visual examination with the wide-field binocular tube of the TIRF microscope (Fig. 4.3B). Although such high levels of expression and crowding of motors on microtubules hinders the observation of individual motility events, these cells are useful for finding the exact focal plane and fine-tuning TIRF excitation. Cells with lower expression levels are more difficult to identify under low-power excitation conditions, but imaging with the EMCCD camera at 200 ms integration time clearly reveals transfected kinesin motors within the cellular background fluorescence (Fig. 4.3C and D). Notice that the autofluorescence background of the cells helps identify cell boundaries (Fig. 4.3B).

5.6. Recording image sequences

1. Once a cell with proper expression level is identified, the beam diameter of the incident laser illumination is adjusted to the desired imaging area (~30 μm diameter) with the TIRF field-iris. This further limits unnecessary photobleaching and cell damage.
2. To accurately track single motor motility events with sufficient resolution and to clearly distinguish diffusion events, higher laser powers (0.1–0.5 mW) are used and long image sequences (>300 frames) at frame rates between 10 and 100 Hz are recorded with the EMCCD camera.
3. Depending on the expression level, multiple image sequences can be taken from the same area of a cell. Typically we wait a few minutes between image series to allow enough unbleached motor molecules to move/diffuse into the field of view.

5.7. Identifying individual single motor events in live cells

Single motor motility events are identified as diffraction-limited fluorescent spots (~250 nm in diameter) that undergo unidirectional processive movement. In live-cell imaging, a large number of motility events can be used to identify microtubule tracks. We find such microtubule tracks by calculating standard deviation maps (SD maps) of the image series (see below). Overlaying individual frames from the image series on the SD map allows the

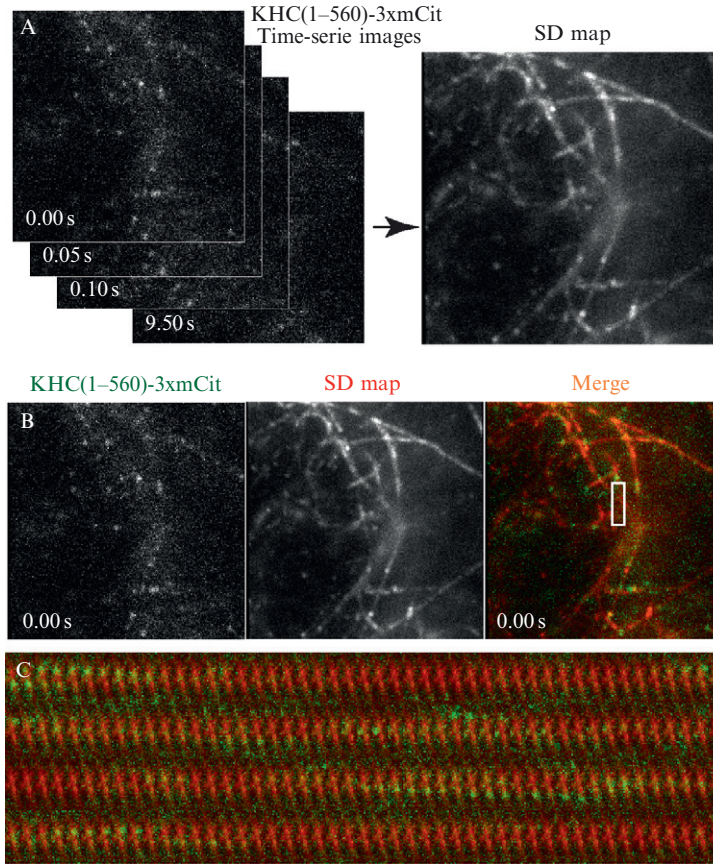

Figure 4.4 Standard deviation map. (A) A 9.5 s long image series containing 190 frames was calculated as described in the text. (B) Overlaying raw images with a SD map helps identify individual motility events. (C) Kymograph of the boxed region in (B) shows that numerous motility events occur on a highlighted track in the SD map.

alignment of motility events with microtubule tracks and provides additional criteria to define single kinesin motility events (Fig. 4.4B and C).

5.8. SD maps

The purpose of the standard deviation map (SD map) is to determine the location of microtubule tracks and to calculate how frequently motors bind to and move along particular tracks (relative to other tracks) (Fig. 4.4). In live-cell imaging sequences, four main noise sources degrade the motor's fluorescence signal: camera (readout) noise, cellular autofluorescence, diffusing fluorescent motors, and out-of-focus background fluorescence. These noise

sources fluctuate randomly and therefore generate background fluorescence whereas the fluorescence intensity of the motor should be significant relative to these noise sources. Thus, motor motility events should contribute significantly to the fluorescence intensity fluctuation (or standard deviation) of a particular pixel of interest. We calculated SD maps (Fig. 4.4A) by determining the statistical intensity variation of each pixel location from the raw images of a video sequence (an image stack) and plotting them in the form of an image. In brief, for an image stack containing Z slices of images with $M \times N$ pixels, the intensity (I) of each pixel in the standard deviation map was calculated with ImageJ (ZProjector_StandardDeviation) as

$$I_{\text{std. dev},[m][n]} = \sqrt{\frac{1}{Z-1}\sum_{k=1}^{Z}\left(I_{[m][n][k]} - \frac{1}{Z}\sum_{k=1}^{z} I_{[m][n][k]}\right)^2}$$

In our work on the possible role of posttranslational modifications of microtubules in regulating cellular transport, analysis of imaging data with SD maps proved extremely helpful in identifying subpopulations of microtubules that are distinguished by different kinesin families to enable targeting of transport events to distinct subcellular domains (Cai *et al.*, 2009).

5.9. High-resolution tracking

To analyze the movement of kinesins with subdiffraction-limited resolution, we use single particle tracking methods (see FIONA in Section 4.5). Given the limited brightness of our fluorescent protein tags, we obtain a spatial resolution of ~20 nm when tracking kinesins at frame rates of 30 Hz (Cai *et al.*, 2007). We implemented FIONA-based particle tracking using 2D Gaussian fitting routines available in MATLAB (The MathWorks, Natick, MA) and ImageJ (NIH, http://rsbweb.nih.gov/ij/).

The accuracy of FIONA depends on a number of experimental parameters, including reduced image quality due to fluorescence background (cellular autofluorescence, freely diffusing fluorescent label) and undesirable photophysical properties of the fluorescent marker (quantum dot blinking, fluorescence photobleaching, self-quenching of multiply-labeled proteins). The fitting routine used to analyze images of a moving, diffraction-limited spot may also be prone to localization errors due to inherent optical aberrations (spherical and chromatic aberration, coma, astigmatism, image distortion, etc.), unclean optical components (especially dust in conjugated imaging planes, such as the CCD chip), and mechanical and thermal drift of the stage and other critical microscope components. For a quantitative comparison of the accuracies and errors associate with various fitting methods, including 2D Gaussian fitting and image cross-correlation, refer

to Cheezum *et al.* (2001). In general, however, experimental methods are now well developed such that the primary limitation for any FIONA-based measurement capable of localizing single, fluorescent molecules is not the diffraction limit imposed by the Rayleigh criterion, but rather the strength (brightness above background) of the signal. Under such conditions photon shot noise dominates all other noise sources (including background fluorescence, pixel effects, and CCD readout noise) limiting the localization analysis (Thompson *et al.*, 2002). Thus, the uncertainty of localizing the center of diffraction-limited spots, ε, is simply a function of the NA, the wavelength of light (λ), and the number of photons collected (N) and well approximated by Greenleaf *et al.* (2007):

$$\varepsilon \cong \frac{\lambda}{2NA\sqrt{N}}$$

6. Summary and Conclusions

Recent advances in imaging and labeling techniques have made it possible to routinely track the movement and distribution of single motor molecules and cytoskeletal proteins in the cytoplasm of mammalian cells. These methods are based on single particle tracking approaches where the centroid position of a label is determined with sub-diffraction-limited resolution. Due to their relatively high brightness, methods based on organelle tracking, gold particles, or aggregates of larger numbers of QDs enable particle tracking with superior spatial and temporal (nanometer and sub-millisecond) resolution, but lack precisely defined labeling stoichiometries and molecular definition that characterize fluorescent protein tags and genetic labels. We expect that the large number of problems remaining in cell biology that hinge on our ability to study the interactions and functions of multiprotein complexes at or close to the single-molecule level *in vivo* will be facilitated by new genetic labeling methods to address remaining limitations, including brightness, photostability, and restricted dye selection. Nonetheless, the existing methods presented in this chapter, which utilize multicolor fluorescence imaging techniques, are bound to impact on many important aspects of modern cell biology and will define the complex interactions of molecular motors and the cytoskeleton.

ACKNOWLEDGMENTS

We apologize that many original contributions could not be cited because of space limitations. Our original work in the area is supported by National Institutes of Health (NIH) grants to KJV (GM070862 and GM083254) and EM (GM076476 and GM083254).

REFERENCES

Alivisatos, A. P., Gu, W. W., and Larabell, C. (2005). Quantum dots as cellular probes. *Ann. Rev. Biomed. Eng.* **7,** 55–76.

Allen, R. D., Allen, N. S., and Travis, J. L. (1981). Video-enhanced contrast, differential interference contrast (AVEC-DIC) microscopy: A new method capable of analyzing microtubule-related motility in the reticulopodial network of Allogromia laticollaris. *Cell Motil.* **1,** 291–302.

Axelrod, D. (2003). Total internal reflection fluorescence microscopy in cell biology. *Methods Enzymol.* **361,** 1–33.

Barak, L. S., and Webb, W. W. (1982). Diffusion of low density lipoprotein–receptor complex on human fibroblasts. *J. Cell Biol.* **95,** 846–852.

Betzig, E., Patterson, G. H., Sougrat, R., Lindwasser, O. W., Olenych, S., Bonifacino, J. S., Davidson, M. W., Lippincott-Schwartz, J., and Hess, H. F. (2006). Imaging intracellular fluorescent proteins at nanometer resolution. *Science* **313,** 1642–1645.

Block, S. M. (2007). Kinesin motor mechanics: Binding, stepping, tracking, gating, and limping. *Biophys. J.* **92,** 2986–2995.

Brady, S. T. (1985). A novel brain ATPase with properties expected for the fast axonal-transport motor. *Nature* **317,** 73–75.

Braslavsky, I., Amit, R., Ali, B. M. J., Gileadi, O., Oppenheim, A., and Stavans, J. (2001). Objective-type dark-field illumination for scattering from microbeads. *Appl. Optics* **40,** 5650–5657.

Cai, D. W., Verhey, K. J., and Meyhofer, E. (2007). Tracking single kinesin molecules in the cytoplasm of mammalian cells. *Biophys. J.* **92,** 4137–4144.

Cai, D., McEwen, D. P., Martens, J. R., Meyhofer, E., and Verhey, K. J. (2009). Single molecule imaging reveals differences in microtubule track selection between Kinesin motors. *PLoS Biol.* **7,** e1000216.

Chang, Y. P., Pinaud, F., Antelman, J., and Weiss, S. (2008). Tracking bio-molecules in live cells using quantum dots. *J. Biophoton.* **1,** 287–298.

Cheezum, M. K., Walker, W. F., and Guilford, W. H. (2001). Quantitative comparison of algorithms for tracking single fluorescent particles. *Biophys. J.* **81,** 2378–2388.

Cherry, R. J. (1992). Keeping track of cell surface receptor. *Trends Cell Biol.* **2,** 242–244.

Churchman, L. S., Okten, Z., Rock, R. S., Dawson, J. F., and Spudich, J. A. (2005). Single molecule high-resolution colocalization of Cy3 and Cy5 attached to macromolecules measures intramolecular distances through time. *Proc. Natl. Acad. Sci. USA* **102,** 1419–1423.

Courty, S., Luccardini, C., Bellaiche, Y., Cappello, G., and Dahan, M. (2006). Tracking individual kinesin motors in living cells using single quantum-dot imaging. *Nano Lett.* **6,** 1491–1495.

Davidson, M. W., and Campbell, R. E. (2009). Engineered fluorescent proteins: Innovations and applications. *Nat. Methods* **6,** 713–717.

Dieterlen, M. T., Wegner, F., Schwarz, S. C., Milosevic, J., Schneider, B., Busch, M., Romuss, U., Brandt, A., Storch, A., and Schwarz, J. (2009). Non-viral gene transfer by nucleofection allows stable gene expression in human neural progenitor cells. *J. Neurosci. Methods* **178,** 15–23.

Dunn, A. R., and Spudich, J. A. (2007). Dynamics of the unbound head during myosin V processive translocation. *Nat. Struct. Mol. Biol.* **14,** 246–248.

Funatsu, T., Harada, Y., Tokunaga, M., Saito, K., and Yanagida, T. (1995). Imaging of single fluorescent molecules and individual ATP turnovers by single myosin molecules in aqueous solution. *Nature* **374,** 555–559.

Gaietta, G., Deerinck, T. J., Adams, S. R., Bouwer, J., Tour, O., Laird, D. W., Sosinsky, G. E., Tsien, R. Y., and Ellisman, M. H. (2002). Multicolor and electron microscopic imaging of connexin trafficking. *Science* **296,** 503–507.

Gelles, J., Schnapp, B. J., and Sheetz, M. P. (1988). Tracking kinesin-driven movements with nanometre-scale precision. *Nature* **331,** 450–453.

Gennerich, A., and Vale, R. D. (2009). Walking the walk: How kinesin and dynein coordinate their steps. *Curr. Opin. Cell Biol.* **21,** 59–67.

Giepmans, B. N., Adams, S. R., Ellisman, M. H., and Tsien, R. Y. (2006). The fluorescent toolbox for assessing protein location and function. *Science* **312,** 217–224.

Greenleaf, W. J., Woodside, M. T., and Block, S. M. (2007). High-resolution, single-molecule measurements of biomolecular motion. *Annu. Rev. Biophys. Biomol. Struct.* **36,** 171–190.

Griffin, B. A., Adams, S. R., and Tsien, R. Y. (1998). Specific covalent labeling of recombinant protein molecules inside live cells. *Science* **281,** 269–272.

Gross, S. P., Tuma, M. C., Deacon, S. W., Serpinskaya, A. S., Reilein, A. R., and Gelfand, V. I. (2002). Interactions and regulation of molecular motors in Xenopus melanophores. *J. Cell Biol.* **156,** 855–865.

Howard, J., Hudspeth, A. J., and Vale, R. D. (1989). Movement of microtubules by single kinesin molecules. *Nature* **342,** 154–158.

Huang, B., Jones, S. A., Brandenburg, B., and Zhuang, X. (2008). Whole-cell 3D STORM reveals interactions between cellular structures with nanometer-scale resolution. *Nat. Methods* **5,** 1047–1052.

Ince, C., Ypey, D. L., Diesselhoff-Den Dulk, M. M., Visser, J. A., De Vos, A., and Van Furth, R. (1983). Micro-CO2-incubator for use on a microscope. *J. Immunol. Methods* **60,** 269–275.

Johnsson, K. (2009). Visualizing biochemical activities in living cells. *Nat. Chem. Biol.* **5,** 63–65.

Jun, Y. W., Sheikholeslami, S., Hostetter, D. R., Tajon, C., Craik, C. S., and Alivisatos, A. P. (2009). Continuous imaging of plasmon rulers in live cells reveals early-stage caspase-3 activation at the single-molecule level. *Proc. Natl. Acad. Sci. USA* **106,** 17735–17740.

Keppler, A., Gendreizig, S., Gronemeyer, T., Pick, H., Vogel, H., and Johnsson, K. (2003). A general method for the covalent labeling of fusion proteins with small molecules in vivo. *Nat. Biotechnol.* **21,** 86–89.

Kinosita, K., Jr., Itoh, H., Ishiwata, S., Hirano, K., Nishizaka, T., and Hayakawa, T. (1991). Dual-view microscopy with a single camera: Real-time imaging of molecular orientations and calcium. *J. Cell Biol.* **115,** 67–73.

Kulic, I. M., Brown, A. E. X., Kim, H., Kural, C., Blehm, B., Selvin, P. R., Nelson, P. C., and Gelfand, V. I. (2008). The role of microtubule movement in bidirectional organelle transport. *Proc. Natl. Acad. Sci. USA* **105,** 10011–10016.

Kural, C., Kim, H., Syed, S., Goshima, G., Gelfand, V. I., and Selvin, P. R. (2005). Kinesin and dynein move a peroxisome in vivo: A tug-of-war or coordinated movement? *Science* **308,** 1469–1472.

Kural, C., Serpinskaya, A. S., Chou, Y. H., Goldman, R. D., Gelfand, V. I., and Selvin, P. R. (2007). Tracking melanosomes inside a cell to study molecular motors and their interaction. *Proc. Natl. Acad. Sci. USA* **104,** 5378–5382.

Kural, C., Nonet, M. L., and Selvin, P. R. (2009). FIONA on Caenorhabditis elegans. *Biochemistry* **48,** 4663–4665.

Kusumi, A., Nakada, C., Ritchie, K., Murase, K., Suzuki, K., Murakoshi, H., Kasai, R. S., Kondo, J., and Fujiwara, T. (2005). Paradigm shift of the plasma membrane concept from the two-dimensional continuum fluid to the partitioned fluid: High-speed single-molecule tracking of membrane molecules. *Annu. Rev. Biophys. Biomol. Struct.* **34,** 351–378.

Laib, J. A., Marin, J. A., Bloodgood, R. A., and Guilford, W. H. (2009). The reciprocal coordination and mechanics of molecular motors in living cells. *Proc. Natl. Acad. Sci. USA* **106,** 3190–3195.

Levi, V., and Gratton, E. (2007). Exploring dynamics in living cells by tracking single particles. *Cell Biochem. Biophys.* **48,** 1–15.
Levi, V., Gelfand, V. I., Serpinskaya, A. S., and Gratton, E. (2006). Melanosomes transported by myosin-V in Xenopus melanophores perform slow 35 nm steps. *Biophys. J.* **90,** L07–L09.
Meyhofer, E., and Howard, J. (1995). The force generated by a single kinesin molecule against an elastic load. *Proc. Natl. Acad. Sci. USA* **92,** 574–578.
Michalet, X., Pinaud, F. F., Bentolila, L. A., Tsay, J. M., Doose, S., Li, J. J., Sundaresan, G., Wu, A. M., Gambhir, S. S., and Weiss, S. (2005). Quantum dots for live cells, in vivo imaging, and diagnostics. *Science* **307,** 538–544.
Nan, X., Sims, P. A., Chen, P., and Xie, X. S. (2005). Observation of individual microtubule motor steps in living cells with endocytosed quantum dots. *J. Phys. Chem. B.* **109,** 24220–24224.
Nan, X. L., Sims, P. A., and Xie, X. S. (2008). Organelle tracking in a living cell with microsecond time resolution and nanometer spatial precision. *Chemphyschem* **9,** 707–712.
Nelson, S. R., Ali, M. Y., Trybus, K. M., and Warshaw, D. M. (2009). Random walk of processive, quantum dot-labeled myosin Va molecules within the actin cortex of COS-7 cells. *Biophys. J.* **97,** 509–518.
Nishiyama, M., Muto, E., Inoue, Y., Yanagida, T., and Higuchi, H. (2001). Substeps within the 8-nm step of the ATPase cycle of single kinesin molecules. *Nat. Cell Biol.* **3,** 425–428.
Okada, C. Y., and Rechsteiner, M. (1982). Introduction of macromolecules into cultured mammalian cells by osmotic lysis of pinocytic vesicles. *Cell* **29,** 33–41.
Park, H., Hanson, G. T., Duff, S. R., and Selvin, P. R. (2004). Nanometre localization of single ReAsH molecules. *J. Microsc.* **216,** 199–205.
Ray, S., Meyhofer, E., Milligan, R. A., and Howard, J. (1993). Kinesin follows the microtubule's protofilament axis. *J. Cell Biol.* **121,** 1083–1093.
Reinhard, B. M., Siu, M., Agarwal, H., Alivisatos, A. P., and Liphardt, J. (2005). Calibration of dynamic molecular rule based on plasmon coupling between gold nanoparticles. *Nano Lett.* **5,** 2246–2252.
Rong, G. X., Wang, H. Y., Skewis, L. R., and Reinhard, B. M. (2008). Resolving sub-diffraction limit encounters in nanoparticle tracking using live cell plasmon coupling microscopy. *Nano Lett.* **8,** 3386–3393.
Ross, J., Buschkamp, P., Fetting, D., Donnermeyer, A., Roth, C. M., and Tinnefeld, P. (2007). Multicolor single-molecule spectroscopy with alternating laser excitation for the investigation of interactions and dynamics. *J. Phys. Chem. B.* **111,** 321–326.
Roy, R., Hohng, S., and Ha, T. (2008). A practical guide to single-molecule FRET. *Nat. Methods* **5,** 507–516.
Sako, Y., and Yanagida, T. (2003). Single-molecule visualization in cell biology. *Nat. Rev. Mol. Cell Biol.* SS1–SS5.
Salmon, E. D., and Tran, P. (1998). High-resolution video-enhanced differential interference contrast (VE-DIC) light microscopy. *Methods Cell Biol.* **56,** 153–184.
Saxton, M. J., and Jacobson, K. (1997). Single-particle tracking: Applications to membrane dynamics. *Annu. Rev. Biophys. Biomol. Struct.* **26,** 373–399.
Schliwa, M., and Woehlke, G. (2003). Molecular motors. *Nature* **422,** 759–765.
Schmidt, T., Schutz, G. J., Baumgartner, W., Gruber, H. J., and Schindler, H. (1996). Imaging of single molecule diffusion. *Proc. Natl. Acad. Sci. USA* **93,** 2926–2929.
Shaner, N. C., Steinbach, P. A., and Tsien, R. Y. (2005). A guide to choosing fluorescent proteins. *Nat. Methods* **2,** 905–909.
Shaner, N. C., Lin, M. Z., McKeown, M. R., Steinbach, P. A., Hazelwood, K. L., Davidson, M. W., and Tsien, R. Y. (2008). Improving the photostability of bright monomeric orange and red fluorescent proteins. *Nat. Methods* **5,** 545–551.

Shubeita, G. T., Tran, S. L., Xu, J., Vershinin, M., Cermelli, S., Cotton, S. L., Welte, M. A., and Gross, S. P. (2008). Consequences of motor copy number on the intracellular transport of Kinesin-1-driven lipid droplets. *Cell* **135,** 1098–1107.

Simon, S. M. (2009). Partial internal reflections on total internal reflection fluorescent microscopy. *Trends Cell Biol.* **19,** 661–668.

Snapp, E. L. (2009). Fluorescent proteins: A cell biologist's user guide. *Trends Cell Biol.* **19,** 649–655.

Svoboda, K., Schmidt, C. F., Schnapp, B. J., and Block, S. M. (1993). Direct observation of kinesin stepping by optical trapping interferometry. *Nature* **365,** 721–727.

Thompson, R. E., Larson, D. R., and Webb, W. W. (2002). Precise nanometer localization analysis for individual fluorescent probes. *Biophys. J.* **82,** 2775–2783.

Tokunaga, M., Imamoto, N., and Sakata-Sogawa, K. (2008). Highly inclined thin illumination enables clear single-molecule imaging in cells. *Nat. Methods* **5,** 159–161.

Vale, R. D., Reese, T. S., and Sheetz, M. P. (1985). Identification of a novel force-generating protein, kinesin, involved in microtubule-based motility. *Cell* **42,** 39–50.

Visscher, K., Schnitzer, M. J., and Block, S. M. (1999). Single kinesin molecules studied with a molecular force clamp. *Nature* **400,** 184–189.

Walter, N. G., Huang, C. Y., Manzo, A. J., and Sobhy, M. A. (2008). Do-it-yourself guide: How to use the modern single-molecule toolkit. *Nat. Methods* **5,** 475–489.

Watanabe, N., and Mitchison, T. J. (2002). Single-molecule speckle analysis of actin filament turnover in lamellipodia. *Science* **295,** 1083–1086.

Yildiz, A., Forkey, J. N., McKinney, S. A., Ha, T., Goldman, Y. E., and Selvin, P. R. (2003). Myosin V walks hand-over-hand: Single fluorophore imaging with 1.5-nm localization. *Science* **300,** 2061–2065.

Yildiz, A., Tomishige, M., Vale, R. D., and Selvin, P. R. (2004). Kinesin walks hand-over-hand. *Science* **303,** 676–678.